

# Power of Confinement: Adsorbate Dynamics on Nanometer-Scale Exposed Facets

Zhihai Cheng,<sup>†</sup> Miaomiao Luo,<sup>†</sup> Jonathan Wyrick,<sup>‡</sup> Dezheng Sun,<sup>‡</sup> Daeho Kim,<sup>†</sup> Yeming Zhu,<sup>‡</sup> Wenhao Lu,<sup>†</sup> Kwangmoo Kim,<sup>§</sup> T. L. Einstein,<sup>§</sup> and Ludwig Bartels<sup>\*,†,‡</sup>

<sup>†</sup>Department of Chemistry and <sup>‡</sup>Department of Physics, University of California-Riverside, Riverside, California 92521 and <sup>§</sup>Department of Physics, University of Maryland, College Park, Maryland 20742-4111

**ABSTRACT** The diffusion and arrangements of CO adsorbates within nanometer-scale pores on a copper surface are investigated by low-temperature scanning tunneling microscopy. In contrast to extended terraces, confinement stabilizes dislocation lines that expose more than one-fourth of the adsorbate population to potentially more reactive adsorption configurations. Confinement allows correlation between adsorbate diffusivity and the number of adsorbates in the pore. A marked increase is found that coincides with the absence of dense films on the exposed facets. In combination, we find that in confinement CO molecules are much more likely to be at adsorption sites that allow lateral access, in contrast to the dense and uniform films on extended terraces.

**KEYWORDS** Scanning tunneling microscopy, diffusion, nanoparticles, molecular network

The diffusive behavior of adsorbates has generally been studied on extended terraces, that is, not under lateral confinement, mainly due to experimental impediments, yet metal clusters with nanoscopic facets have considerable technological relevance, for instance as supported metal catalysts for applications ranging from the (petro-)chemical industry to emission control. For the study of the dynamics of adsorbates on nanoscale clusters, it would be ideal if arrays of atomically identical ones could be formed. Absent this possibility we utilize a Cu(111) substrate covered with a self-assembled anthraquinone network. This network sustains subsequent deposition of CO molecules and confines their diffusion into pores of  $\sim 4$  nm in size, where they can be imaged and studied in detail.

The pores have a similar size as the facets expected on catalytic nanoclusters; in particular, studies on gold have shown that its activity increases enormously if dispersed in this size regime.<sup>2,3</sup> Conventionally, the high activity of nanoparticles, as compared to the surfaces of bulk metals, is attributed partly to the high surface to volume ratio at high dispersion, and partly to support-metal interactions and to the abundance of surface defect sites such as step-/facet-edges and -kinks.<sup>4</sup> While the exposed copper facets of our network probably have little besides their size in common with catalytic nanoparticles, they nevertheless open for study the kind of effects that lateral confinement may have on the dynamics of adsorbates, at least in a phenomenological manner; a survey of them is the objective of this study.

Several previous publications addressed the dynamics of adsorbates at metal surfaces and their interaction with one another. They include measurements of the dynamics of

benzene molecules,<sup>5,6</sup> reactive mixtures,<sup>7,8</sup> hydrogen atoms,<sup>9</sup> and CO molecules.<sup>10–15</sup> Also, the insertion of atoms or molecules into molecular surface networks has been studied previously.<sup>16–21</sup> What makes our study novel is the confined nature of the adsorbates that allows us to study how molecules behave when their support is not a large, clean, and inert terrace.<sup>22</sup>

We use CO as our test molecule because abundant data on its surface behavior is available: CO molecules adsorb upright atop Cu(111) substrate atoms. They are imaged in scanning tunneling microscopy (STM) as protrusions or indentations, depending on whether the STM tip is decorated with a CO atom at its apex or not, respectively.<sup>23</sup> At sufficient coverage, CO adsorbates form an ordered  $(\sqrt{3} \times \sqrt{3})R30^\circ$  overlayer; large islands of this superstructure have been observed in previous STM studies.<sup>24</sup> In our model system there are 186 exposed atop adsites in each 4 nm pore, allowing a maximum occupation in the exposed facet of 62 CO molecules in a dense  $(\sqrt{3} \times \sqrt{3})R30^\circ$  adlayer.

Initial sample preparation involves the usual sequence of sputtering and annealing, followed by cooling to liquid nitrogen temperatures. The anthraquinone pattern is created by deposition of the molecule onto the cryogenic sample followed by annealing to room temperature. After subsequent cooling to  $\sim 40$  K, CO is deposited through a leak valve.

Deposition of CO molecules into an anthraquinone honeycomb network does not alter the pore shape. With careful dosage we obtain a CO coverage very close to a complete  $(\sqrt{3} \times \sqrt{3})R30^\circ$  overlayer, which is visible inside the pores (Figure 1b–d). Moreover, we find on the exposed facets a dislocation line, which is constantly present yet persistently shifting position. The Supporting Information shows a movie. This differs from the behavior of CO films on extended terraces, where the  $(\sqrt{3} \times \sqrt{3})R30^\circ$  is observed over large

\* To whom correspondence should be addressed. E-mail: Ludwig.Bartels@ucr.edu.

Received for review: 06/22/2010

Published on Web: 08/03/2010

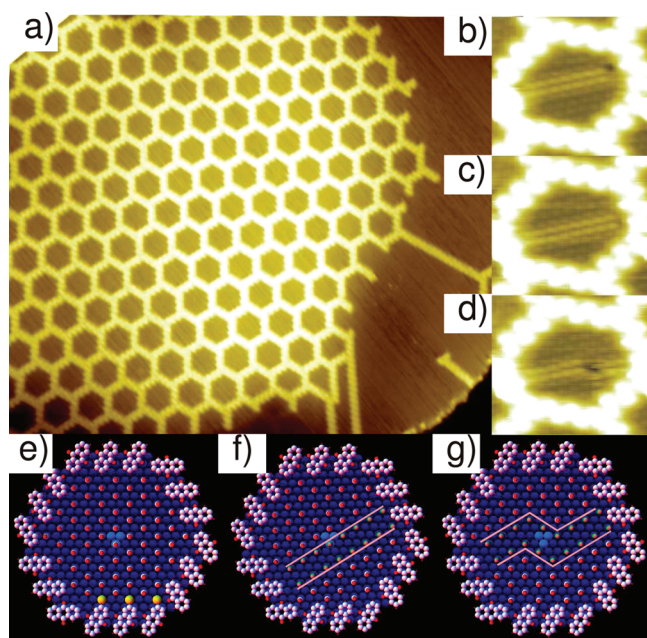


**FIGURE 1.** (a) Array of atomically defined pores on Cu(111) formed by deposition of anthraquinone according to ref 1. Image parameters, 83 nm  $\times$  73 nm; bias,  $-2.53$  V; current, 50 pA; temperature, 90 K. (b–d) Images from a supporting movie of a dislocation line moving in confinement. Image parameters: bias  $-2.40$  V; current 44 pA; temperature, 24 K. e,f) The  $(\sqrt{3} \times \sqrt{3})R30^\circ$  adlayer can be anchored at any one of the three atoms at the center of the exposed facet (light blue). In each case, one facet edge is decorated differently than the remaining two of the same kind (yellow in e). This can be alleviated, if a dislocation line is induced in the pore (f). In both cases, the same number of molecules fit inside the pore. (g) Model of a kink in a dislocation line similar to the STM image of panel d.

areas and dislocation lines (i.e., antiphase domain boundaries) are expelled to the edge.<sup>24</sup> What is the origin of this effect?

Each exposed facet is centered around a substrate hollow site, allowing three equivalent atop adsites (light blue in Figure 1e) to anchor the CO  $(\sqrt{3} \times \sqrt{3})R30^\circ$  pattern, thus spanning three equivalent overlayer sublattices. The facet edges consist of two alternating sets of three equivalent sides, much as any hexagonal fcc island is surrounded by steps with alternating (111) and (100) facets. One of the sets of sides is equally decorated with CO molecules no matter which central substrate atom anchors the overlayer. Of the other set of sides, however, only two are covered intimately, leaving open space near the third side (yellow in Figure 1e).

The open space can be avoided if the CO adlayer is imperfect; a dislocation line in the overlayer allows placement of adsorbates at all sides of the second set equivalently. Consequently, the confined adlayer is under competition between forming the structure found on extended surfaces and incorporation of a dislocation line that permits equal filling of the edge sites, that is, providing optimal edge interaction at the expense of intermolecular interaction. In both cases, the same number of CO molecules fit onto the exposed facet. The observation of the persistence of the

dislocation lines indicates that the interactions at the adlayer edge are dominant over those within the adlayer.

Imaging 75 setups of one dislocation line at 24 K, we find that in  $\sim 40\%$  of the cases a kink is present in the line. A dislocation typically affects 16 molecules (8 per side); a kink in the double line increases this number by 2 along the dislocation line (Figure 1g). Analyzing the measured fraction of kinked lines using the Boltzmann equation and taking into account the degeneracy of the various possible kinked configurations, we estimate a kink energy of  $6.1 \pm 0.3$  meV and a total energetic cost of the entire dislocation line of  $\sim 0.05$  eV. For three molecules, the edge-interaction is improved by the dislocation line (yellow in Figure 1e). This yields a lower boundary of the edge interaction of  $\sim 0.02$  eV per molecule, a considerable energy compared to, for example, the CO diffusion barrier of 0.075 eV.<sup>13</sup>

The presence of the dislocation can potentially affect the chemical reactivity of the film markedly; molecules affected by a dislocation line have a nearest neighbor configuration that allows more ready access to them as well as the underlying substrate. The number of molecules affected by the dislocation scales linearly with the size of the facet, whereas the total number of molecules scales quadratically, indicating that the smaller the facet size, the more pronounced this effect. For the 4 nm facets studied here, more than one-fourth of the adsorbates (16 out of 62) are directly affected by the dislocation line, significantly greater than on extended terraces.

The constant motion of the dislocation lines well below 30 K contrasts substantially with the behavior of individual CO molecules on Cu(111), whose diffusion starts only at  $\sim 33$  K.<sup>13</sup> Is this effect limited to dislocation lines? Preparing films of slightly lower coverage with facets that have a small number of vacancies in their  $(\sqrt{3} \times \sqrt{3})R30^\circ$  coverage (Figure 2a,b), we observe rapid motion at similarly low temperature. The Supporting Information shows a movie. While increased diffusivity at high coverage has been observed in the past, to our knowledge it has not yet been quantified except at very low concentration<sup>13</sup> and for direct neighbors.<sup>12,25,26</sup> The confined nature of our exposed facets allows us to monitor the diffusion rate for a fixed number-density of molecules. The dotted line of Figure 3 shows the diffusivity from a few molecules per pore (Figure 2e,f) up to the point at which the  $(\sqrt{3} \times \sqrt{3})R30^\circ$  adlayer is one-third complete and site blocking becomes important (Figure 2c,d). While data points for coverages up to 6 molecules on the exposed facet were measured at 27 K, diffusion at higher coverages was too rapid at this temperature; the data point for 21 molecules per pore was measured at 22 K and scaled according to the Arrhenius parameters of ref 13. The dotted line represents an exponential fit of the diffusivity.

A detailed look at the STM images indicates that the diffusivity depends not only on the number of molecules on the exposed facet but also on the position of the molecules within that facet. Generally, molecules tend to move less if

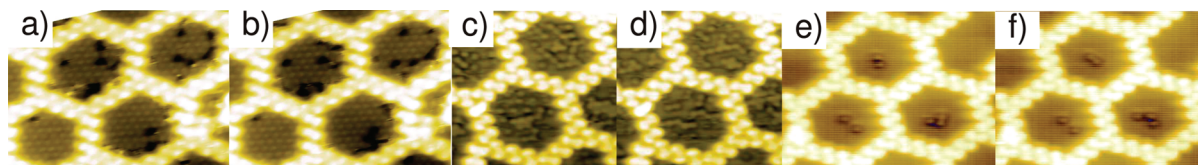


FIGURE 2. Images from STM movies showing the diffusion of (a,b) vacancies in a  $(\sqrt{3} \times \sqrt{3})R30^\circ$  CO coverage in confinement (image parameters, 12 nm  $\times$  9 nm; bias,  $-1.23$  V; current, 120 pA, temperature, 23 K). (c,d) Twenty to twenty-two CO molecules on each exposed facet (image parameters, 8 nm  $\times$  8 nm; bias,  $-0.72$  V; current, 60 pA, temperature, 22 K). (e,f) Two and three CO molecules in confinement (image parameters, 12 nm  $\times$  9 nm; bias,  $-2.67$  V; current, 100 pA, temperature, 27 K).

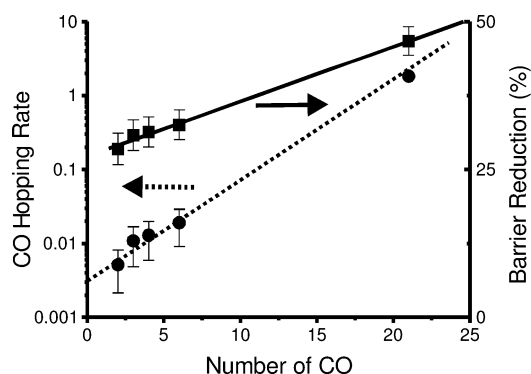


FIGURE 3. Dotted line: diffusion rate per molecule as a function of number of molecules on an exposed facet. Solid line: reduction of the diffusion barrier that causes this acceleration under the assumption of a constant diffusion prefactor. All error bars are dominated by the temperature uncertainty of 1 K in our measurements; the statistical error is much smaller than the data markers.

they are closer to the center and more rapidly around the perimeter. Unfortunately, this renders a complete Arrhenius-based evaluation (which would need to separate molecules by location) beyond reasonable effort.

Thermally programmed desorption experiments showed that an increase of the surface coverage can lead to a reduction of the adsorption energy.<sup>4</sup> In the simplest approximation, the diffusion barrier is a constant fraction of the adsorption energy. While this argument justifies a variation of the diffusion barrier with coverage, it provides little indication that the diffusion preexponential factor should vary markedly with it. Fixing the diffusion prefactor at the value for isolated molecules,<sup>15</sup> the variation of the diffusion barrier with coverage can be obtained from the diffusion data (Figure 3, solid line). The adsorption and subdivision of the Cu(111) terrace by the anthraquinone network causes a reduction of the CO diffusion barrier by one-fourth; increasing the coverage inside the pore up to one-third of the  $(\sqrt{3} \times \sqrt{3})R30^\circ$  adlayer reduces the diffusion barrier by another one-fourth. The data suggests a linear fit of the reduction of the barrier as a function of the coverage with a slope of  $(57 \pm 14)\%$ /ML, with 1 ML defined as the complete  $(\sqrt{3} \times \sqrt{3})R30^\circ$  coverage. If the adsorption energy is assumed to be proportional to the diffusion barrier, then its reduction by half indicates a comparable reduction of the adsorption energy. The observation of a linear dependence of the energy reduction on the number density of molecules suggests that its origin is not direct pair interactions (which

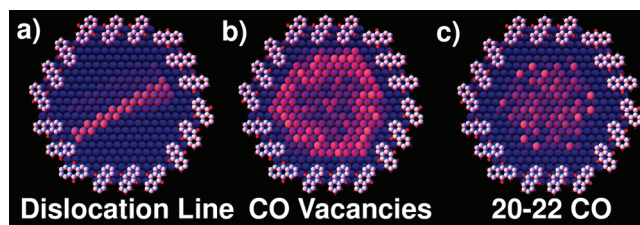


FIGURE 4. Color-coded histograms of CO vacancy/molecule distribution for each of the 186 Cu substrate atoms exposed within an anthraquinone pore. The anthraquinone pore is chiral and 3-fold symmetric, panels b and c are averaged over three equivalent rotational orientations. (a) Dislocation lines are most commonly found to cross the facet center, (b) whereas vacancies are more commonly found around the facet edge. (c) For 20–22 CO molecules, a relatively featureless distribution is observed. Each panel represents the location of >1000 vacancies/molecules.

scale quadratically with coverage) but involves the substrate, potentially both through confinement-induced surface state effects<sup>27–29</sup> or through mediation of trio and higher order interactions.<sup>30</sup> While the effects of site blocking and nearest neighbor interactions prevent us from obtaining experimental data beyond  $1/3$  ML coverage, our results suggest a quite substantial destabilization of the CO molecules in the  $(\sqrt{3} \times \sqrt{3})R30^\circ$  adlayer, well in line with the results discussed in refs 4 and 26.

Following this discussion of the CO dynamics, we finally examine the locations that the molecules/vacancies occupy and the effect of the lateral confinement on them. To this end, we study the distribution of vacancies in coverages like the one shown in Figure 2a–d and of molecules in coverages like shown in Figure 2c,d; movies can be found in the online Supporting Information.

Figure 4a shows the likelihood that the dislocation line of Figure 1b–d occupies different substrate sites in a color-coded histogram. In this context, it is important to realize that although the anthraquinone network appears 6-fold symmetric, due to the 3-fold (and not 6-fold) symmetry of the substrate, every other of its sides comes to rest at different surface locations. The dislocation line generally crosses near the center of the exposed facet thereby connecting dissimilar edges. Consequently, the area showing higher occupation of the dislocation line in the center right of Figure 4a is not equivalent to the area on the center left of the pore line. The sensitivity of the dislocation line to the

geometry of the facet boundary is a testament to the importance of confinement for the spatial distribution of adsorbates.

Figure 4b shows the distribution of vacancies on exposed facets a few molecules short of saturation; bright colors correspond to a high likelihood of finding vacancies. Viewing a large number of movies with coverages similar to Figures 2a,b, we qualitatively observe that the vacancies frequently arrange themselves in rows that originate at the facet edge and often bend back toward the same or an adjacent edge. In the histogram of Figure 4b, this is reflected in a higher probability for vacancies to be found at the edges with a slight preference for one kind of edge and vertex. It is important to realize that in our observation, the vacancies do not segregate from the adlayer, that is, they do not form a closely covered area surrounded by empty space as on extended terraces.<sup>24</sup> Rather the vacancies are interspersed with the adlayer, affecting a far greater fraction of the adlayer molecules and potentially rendering the adlayer more reactive. A statistical analysis of vacancy motion is much more complicated than for adsorbate motion, as in the ( $\sqrt{3} \times \sqrt{3}$ )R30° overlayer “fractional” vacancies (corresponding to molecules adsorbed in antiphase) can combine and molecules can occasionally and intermittently adsorb closer than the  $\sqrt{3}$  spacing, so that the total number of vacancies on an exposed facet is not conserved.

Reducing the coverage to 20–22 molecules on the exposed facet (i.e.,  $\sim 1/3$  of the ( $\sqrt{3} \times \sqrt{3}$ )R30° adlayer), we do not observe aggregation into large islands (Figure 2c,d). Despite the low temperature, only small aggregates of molecules form, with almost every molecule being accessible on the surface from at least one side (see Supporting Information). This is, again, in marked contrast to CO films on extended terraces, where we find extended ( $\sqrt{3} \times \sqrt{3}$ )R30° islands under similar conditions.<sup>24</sup> The distribution of molecules within the exposed facet is relatively featureless; no preferred or avoided regions of adsites can be discerned (Figure 4c).

In summary, we conducted a survey of the effects that nanometer-scale confinement can have on adsorbate dynamics and placement; on small exposed facets we found that adsorbate diffusion increases rather than decreases, resulting in more even and open distributions of adsorbates and adlayer vacancies than found on extended terraces. Even at full coverage, confinement can stabilize dislocation lines that affect a substantial fraction of the molecules in the adlayer (more than one-fourth of them). In combination, these findings suggest that confinement alone can increase the potential for surface reactivity in an adsorbate film: the smaller the facet size (i.e., the smaller a metal nanoparticle that creates it), the more pronounced the mentioned effect.

**Acknowledgment.** This work was supported by joint NSF Grants CHE 07-50334 (T.L.E) and 07-49949 (L.B.), as well as the U.S. Department of Energy Grant DE-FG02-07ER15842

and Air Force Office of Scientific Research Grant FA9550-08-1-0401. T.L.E. had secondary support from NSF MRSEC Grant DMR 05-20471 and ancillary support from CNAM.

**Supporting Information Available.** Movies showing the movement of individual molecules, vacancies, and dislocation lines. This material is available free of charge via the Internet at <http://pubs.acs.org>.

## REFERENCES AND NOTES

- Pawin, G.; Wong, K. L.; Kwon, K. Y.; Bartels, L. *Science* **2006**, *313*, 961–962.
- Haruta, M.; Kobayashi, T.; Sano, H.; Yamada, N. *Chem. Lett.* **1987**, 405–408.
- Chen, M. S.; Goodman, D. W. *Science* **2004**, *306*, 252–255.
- Somorjai, G. A. *Introduction to surface chemistry and catalysis*; Wiley: New York, 1994.
- Mantooth, B. A.; Sykes, E. C. H.; Han, P.; Moore, A. M.; Donhauser, Z. J.; Crespi, V. H.; Weiss, P. S. *J. Phys. Chem. C* **2007**, *111*, 6167–6182.
- Han, P.; Mantooth, B.; Sykes, E.; Donhauser, Z.; Weiss, P. J. *Am. Chem. Soc.* **2004**, *126*, 10787–10793.
- Sachs, C.; Hildebrand, M.; Volkening, S.; Winterlin, J.; Ertl, G. *Science* **2001**, *293*, 1635–1638.
- Hendriksen, B.; Bobaru, S.; Frenken, J. *Surf. Sci.* **2004**, *552*, 229–242.
- Tierney, H. L.; Baber, A. E.; Sykes, E. C. H. *J. Phys. Chem. C* **2009**, *113*, 7246–7250.
- Mitsui, T.; Rose, M. K.; Fomin, E.; Ogletree, D. F.; Salmeron, M. *Phys. Rev. Lett.* **2005**, *94*, No. 036101.
- Briner, B.; Doering, M.; Rust, H.; Bradshaw, A. *Science* **1997**, *278*, 257–260.
- Heinrich, A.; Lutz, C.; Gupta, J.; Eigler, D. *Science* **2002**, *298*, 1381–1387.
- Wong, K. L.; Rao, B. V.; Pawin, G.; Ulin-Avila, E.; Bartels, L. *J. Chem. Phys.* **2005**, *123*, 201102.
- Longwitz, S.; Schnadt, J.; Vestergaard, E.; Vang, R.; Laegsgaard, E.; Stensgaard, I.; Brune, H.; Besenbacher, F. *J. Phys. Chem. B* **2004**, *108*, 14497–14502.
- Kulawik, M.; Rust, H. P.; Heyde, M.; Nilius, N.; Mantooth, B. A.; Weiss, P. S.; Freund, H. J. *Surf. Sci.* **2005**, *590*, L253–L258.
- Theobald, J. A.; Oxtoby, N. S.; Phillips, M. A.; Champness, N. R.; Beton, P. H. *Nature* **2003**, *424*, 1029–1031.
- Stepanow, S.; Lingenfelder, M.; Dmitriev, A.; Spillmann, H.; Delvigne, E.; Lin, N.; Deng, X. B.; Cai, C. Z.; Barth, J. V.; Kern, K. *Nat. Mater.* **2004**, *3*, 229–233.
- Decker, R.; Schlickum, U.; Klappenberger, F.; Zoppellaro, G.; Klyatskaya, S.; Ruben, M.; Barth, J. V.; Brune, H. *Appl. Phys. Lett.* **2008**, *93*, 243102.
- Berner, S.; Corso, M.; Widmer, R.; Groening, O.; Laskowski, R.; Blaha, P.; Schwarz, K.; Goriachko, A.; Over, H.; Gsell, S.; Schreck, M.; Sachdev, H.; Greber, T.; Osterwalder, J. *Angew. Chem., Int. Ed. Engl.* **2007**, *46*, 5115–5119.
- Bartels, L. *Nat. Chem.* **2010**, *2*, 87–95.
- Otero, R.; Rosei, F.; Naitoh, Y.; Jiang, P.; Thostrup, P.; Gourdon, A.; Laegsgaard, E.; Stensgaard, I.; Joachim, C.; Besenbacher, F. *Nano Lett* **2004**, *4*, 75–78.
- Kulawik, M.; Rust, H.-P.; Heyde, M.; Nilius, N.; Mantooth, B. A.; Weiss, P. S.; Freund, H.-J. *Surf. Sci.* **2005**, *590*, L53.
- Bartels, L.; Meyer, G.; Rieder, K. *Appl. Phys. Lett.* **1997**, *71*, 213–215.
- Bartels, L.; Meyer, G.; Rieder, K. *Surf. Sci.* **1999**, *432*, L621–L626.
- Repp, J.; Moresco, F.; Meyer, G.; Rieder, K.; Hyldgaard, P.; Persson, M. *Phys. Rev. Lett.* **2000**, *85*, 2981–2984.
- Shan, B.; Zhao, Y. J.; Hyun, J.; Kapur, N.; Nicholas, J. B.; Cho, K. *J. Phys. Chem. C* **2009**, *113*, 6088–6092.
- Heller, E.; Crommie, M.; Lutz, C.; Eigler, D. *Nature* **1994**, *369*, 464–466.
- Fiete, G. A.; Heller, E. J. *Rev. Mod. Phys.* **2003**, *75*, 933–948.
- Lobo-Checa, J.; Matena, M.; Muller, K.; Dil, J. H.; Meier, F.; Gade, L. H.; Jung, T. A.; Stohr, M. *Science* **2009**, *325*, 300–303.
- Hyldgaard, P.; Einstein, T. L. *Europhys. Lett.* **2002**, *59*, 265–271.